Int J Physiol Pathophysiol Pharmacol 2024;16(3):55-76
www.ijppp.org /ISSN:1944-8171/IJPPP0155908

Original Article

Patterns of connexin36 and eGFP reporter expression among motoneurons in spinal sexually dimorphic motor nuclei in mouse

Prabhisha Silwal, Pratyaksh Singhal, Joanne MM Senecal, Julie EM Senecal, Bruce D Lynn, James I Nagy

Department of Physiology and Pathophysiology, Rady Faculty of Health Sciences, Max Rady College of Medicine, University of Manitoba, Winnipeg, Manitoba R3E 0J9, Canada

Received February 14, 2024; Accepted May 6, 2024; Epub June 15, 2024; Published June 30, 2024

Abstract: Background: Sexually dimorphic spinal motoneurons (MNs) in the dorsomedial nucleus (DMN) and dorsolateral nucleus (DLN) as well as those in the cremaster nucleus are involved in reproductive behaviours, and the cremaster nucleus additionally contributes to testicular thermoregulation. It has been reported that MNs in DMN and DLN are extensively linked by gap junctions forming electrical synapses composed of connexin36 (Cx36) and there is evidence that subpopulation of MNs in the cremaster nucleus are also electrically coupled by these synapses. Methodology: We used immunofluorescence methods to detect enhanced green fluorescent protein (eGFP) reporter for Cx36 expression in these motor nuclei. Results: We document in male mice that about half the MNs in each of DMN and DLN express eGFP, while the remaining half do not. Further, we found that the $eGFP^+$ vs. $eGFP^-$ subsets of MNs in each of these motor nuclei innervate different target muscles; $eGFP^+$ MNs in DMN and DLN project to sexually dimorphic bulbocavernosus and ischiocavernosus muscles, while the $eGFP^-$ subsets project to sexually non-dimorphic anal and external urethral sphincter muscles. Similarly, $eGFP^+$ vs. $eGFP^-$ cremaster MNs were found to project to anatomically distinct portions of the cremaster muscle. By immunofluorescence, nearly all motoneurons in both DMN and DLN displayed punctate labelling for Cx36, including at $eGFP^+/eGFP^+$, $eGFP^+/eGFP^-$ and $eGFP^-/eGFP^-$ cell appositions. Conclusions: Most if not all motoneurons in DMN and DLN are electrically coupled, including sexually dimorphic and non-dimorphic motoneurons with each other, despite absence of eGFP reporter in the non-dimorphic populations in these nuclei that have selective projections to sexually non-dimorphic target muscles.

Keywords: Neuronal gap junctions, connexin36, electrical synapses, sexually dimorphic muscles, bulbocavernosus and ischiocavernosus muscles, external urethral and external anal sphincter, $Cx36^{BAC}$-eGFP mice

Introduction

Electrical synapses formed by gap junctions composed of intercellular communicating channels consisting largely of the gap junction-forming protein connexin36 (Cx36) are present and densely to moderately concentrated in nearly every major structure in the mammalian brain [1-4]. These synapses allow direct electrical transmission or electrical coupling (e-coupling) between neurons [5], contribute to a wide range of integrative capabilities in neural networks in which they are embedded [4, 6, 7], and occur at a variety of neuronal subcellular sites [2, 8-15]. Investigations of electrical synapses in mammalian brain have led to an understanding of the functional importance of these structures in neuronal circuitry of higher vertebrates, particularly in conferring synchronization of neuronal firing in a network of e-coupled cells, which is a widespread feature of neuronal activity in the brain [16-21].

Diverse populations of neurons in the spinal cord are also richly endowed with electrical synapses based on widespread distribution of fluorescent protein reporter for Cx36 expression [22-24], and there has been some progress in understanding some of the physiological roles of electrical synapses in modulating neuronal activity in the spinal neural systems [25-29]. Spinal cord neurons in which evidence for e-coupling has been reported in adult rats and mice include sexually dimorphic motoneurons

https://doi.org/10.62347/OGWV9376

(MNs) in the dorsomedial motor nucleus (DMN; a.k.a., spinal nucleus of the bulbocavernosus) and the dorsolateral motor nucleus (DLN) located in the lower lumbar (L) region (i.e., L5-L6) [30-32]. Another set includes MNs in the sexually dimorphic cremaster motor nucleus located in the upper lumbar spinal cord at the L1-L2 level [33]. These motor nuclei are considered to be sexually dimorphic based on the relatively greater numbers, larger size and responsiveness to circulating androgens of their MNs, and differential degrees of development of the muscles they innervate in males vs. females [34-39]. Subsets of MNs in both the DMN and DLN innervate two distinct groups of striated muscles located in the pelvic floor [38, 40]. Those in DLN project to ischiocavernosus muscle as well as striated muscle forming the external urethral sphincter around the neck of the urinary bladder, while those in the DMN project to bulbocavernosus (a.k.a., bulbospongiosus) muscle as well as striated muscle forming the external anal sphincter. Similarly, cremaster MNs project to the single cremaster muscle, which is nevertheless segregated into a larger portion enveloping the testes and a separate smaller portion surrounding the spermatic cord. In mammals, both portions of the cremaster muscle are essential for providing thermoregulation of the testes [41-43], while the larger portion in addition performs in elevation and protection of the testes [44]. It is generally accepted that MNs in both the upper and lower lumbar sexually dimorphic motor nuclei contribute to various parameters of sexual behavior, including erectile and ejaculatory functions during copulation [41, 45-49].

Spinal sexually dimorphic motor nuclei appear to be remarkably complex in their organization of peripheral projections to target muscles and in the functional interrelationships of their constituent MNs, including perhaps the organization of e-coupling within these nuclei. Indeed, using transgenic mice in which enhanced green fluorescent protein (eGFP) serves as a reporter for Cx36 expression as detected by immunofluorescence labelling of this protein, we recently reported that MNs in the cremaster nucleus are heterogeneous with respect to their eGFP expression, suggesting the presence of both e-coupled and non-coupled MN populations in this nucleus. Here, we document similar heterogeneity in eGFP expression among MNs in the sexually dimorphic DMN and DLN, examine the target muscle projections of these distinct MN populations as well as those in the cremaster nucleus, and evaluate patterns of Cx36 expression as detected by its immunofluorescence localization among MNs in the lower lumbar sexually dimorphic motor nuclei.

Materials and methods

Animals and antibodies

Adult male C57BL/6-129SvEv ($Cx36^{BAC}$::eGFP) transgenic mice (n = 24, 1-2 months of age, 25-29 g in weight) and matching female counterparts (n = 6) were obtained from a colony at the University of Manitoba established with breeding pairs from the UC Davis Mutant Mouse Regional Resource Center (Davis, CA, USA; see also http://www.gensat.org/index.html). Mice were selected by genotyping for expression of bacterial artificial chromosome (BAC) driven expression of eGFP under the Cx36 promoter. Animals were housed under controlled temperature and humidity on a 12:12 hr light/dark cycle and were provided with standard lab chow and tap water ad libitum. Considerations were taken to minimize animal stress and the number of animals used in all procedures. Animals were obtained from the Central Animal Care Services at the University of Manitoba and utilized according to approved protocols by the Central Animal Care Committee of the University of Manitoba. Tissues from these animals were typically obtained between 10:00 am to 1:00 pm.

For immunofluorescence labelling of target proteins in neurons, various combinations of seven commercially available primary antibodies were used. **Table 1** contains the relevant information, including the type (polyclonal or monoclonal), species of origin, commercial source, catalog number designation and dilutions utilized during incubations with tissue sections. Our prior investigations of mammalian CNS using $Cx36^{BAC}$::eGFP mice revealed that many neurons and their processes positively labelled for eGFP were also decorated with punctate Cx36 labelling [23, 33, 50], a finding that supports eGFP expression in most, though perhaps not all, neurons as an indicator of coincident Cx36 expression. In these studies, Cx36 labelling in different CNS regions, including the spinal cord, was detected using a mouse monoclonal anti-

Table 1. The primary antibodies used for labelling in immunofluorescence experiments with their respective type (monoclonal or polyclonal), host species, commercial source, catalogue number, and dilution for use

Primary antibody	Type	Host species	Commercial source*	Catalogue number	Dilution
Cx36	Monoclonal	Mouse	ThermoFisher	39-4200	1:600
eGFP	Monoclonal	Rabbit	ThermoFisher	G10362	1:100
eGFP	Polyclonal	Chicken	Aves	GFP-1010	1:1000
Peripherin	Polyclonal	Chicken	MilliporeSigma	Ab9282	1:500
vAChT	Polyclonal	Guinea pig	Synaptic Systems	139105	1:1000
ChAT	Polyclonal	Goat	MilliporeSigma	Ab144P	1:600

*Locations of Commercial sources: ThermoFisher Scientific, Rockford, IL, USA; Aves Labs Inc., Davis, CA, USA; MilliporeSigma, Burlington, MA, USA; ImmunoStar, Hudson, WI, USA; Synaptic Systems, Goettingen, DE.

body (Cat. No. 39-4200, ThermoFisher, Rockford, IL, USA) raised against Cx36, whose specificity has been established by showing absence of punctate Cx36 labeling in Cx36 null mice [32, 33, 51, 52]. All secondary antibodies used were raised in donkey and included: Cy3-conjugated anti-guinea pig, which was used at a dilution of 1:600 (Jackson ImmunoResearch Laboratories, West Grove, PA, USA); and Alexa488-conjugated anti-rabbit, Alexa488-conjugated anti-chicken, Alexa555-conjugated anti-goat, Alexa555-conjugated anti-mouse and Alexa555-conjugated anti-rabbit antibodies that were used at a dilution of 1:1000 (Molecular Probes, Eugene, OR, USA). Primary and secondary antibody dilutions were prepared in TBST (50 mM Tris-HCl, pH 7.6), 1.5% sodium chloride 0.3% Triton X-100 (Sigma-Aldrich Corp., St. Louis, MO, USA) containing 10% normal donkey serum (NDS; Jackson ImmunoResearch Laboratories, USA).

Tissue preparation

Mice were sacrificed with an anesthetic overdose of 3 ml/kg equithesin and then transcardially perfused with 0.1-0.2 ml per gram body weight of pre-fixative composed of ice-cold 50 mM sodium phosphate buffer, pH 7.4, 0.9% NaCl, 0.1% sodium nitrite and 1 unit/ml heparin, and then with 40 ml of ice-cold fixative containing 0.16 M sodium phosphate, pH 7.1, 0.2% picric acid and 4% formaldehyde (Electron Microscopy Sciences, Hatfield, PA, USA). As previously discussed [23], the simultaneous immunolabelling of Cx36 and eGFP is challenging as optimal detection of Cx36 requires a weaker 1-2% formaldehyde fixative, while eGFP immunofluorescence is poor under such weak fixation conditions. Here, to accomplish co-immunolabelling of these proteins in spinal cord MNs, some mice were transcardially perfused with a formaldehyde/glyoxal fixative composed of 9% (w/v) glyoxal, 8% (w/v) acetic acid, 0.4% (w/v) ethanol and 1% (w/v) formaldehyde, pH 5 with NaOH, as described with modifications [53-55]. The spinal cords of animals were dissected with L1 to L6 roots intact, which assisted in consistently isolating L5-L6 segments containing DMN and DLN motor nuclei in the ventral horn. The bulbospongiosus muscle, ischiocavernosus muscle, external urethral sphincter, external anal sphincter, cremaster muscle, and spermatic cord were dissected using approaches as described [56, 57]. All dissected tissues were post-fixed at 4°C for 1 hr in the same fixative and then stored for 24-48 hrs in cryoprotectant solution consisting of 10% sucrose, 25 mM sodium phosphate buffer, pH 7.4 and 0.1% sodium azide. To prepare the tissue for sectioning, lower lumbar segments (L5-L6) and muscles were embedded with OCT compound (VWR International, PA, USA), flash frozen and then transferred to a cryostat where tissue was sectioned horizontally at a thickness of fifteen µm. Sections were collected on gelatinized glass slides and stored at -35°C before use.

Immunofluorescence labelling

For immunofluorescence labelling procedures, sections mounted on slides were retrieved from storage, washed for 20 min in TBST and primary antibodies diluted in TBST supplemented with 10% NDS were applied. After overnight incubation at 4°C the slides were rinsed at room temperature with TBST (3 × 20 min) and then incubated at room temperature for 1.5 hrs with appropriate combinations of secondary

antibodies diluted in TBST with NDS. Slides were washed with TBST (1 × 20 min), with 50 mM Tris-HCl buffer, pH 7.4 (2 × 15 min), coverslipped with Fluoromount G anti-fade medium (SouthernBiotech, Birmingham, AL, USA) and then stored at -20°C. Whenever feasible, the immunolabelling of eGFP in tissue sections was amplified by utilizing a primary antibody solution that included two distinct species of anti-eGFP antibodies: one generated in rabbit and the other in chicken. These anti-eGFP primary antibodies were used alongside other primary antibodies and detected using anti-chicken and anti-rabbit secondary antibodies conjugated to the fluorophore Alexa488.

A Zeiss Imager Z2 fluorescence microscope and Zeiss Zen software (Carl Zeiss Canada, Toronto, ON, Canada) were used to capture fluorescence images from tissue samples. A Zeiss LSM710 laser scanning confocal microscope with Zen image capture and analysis software was utilized when higher resolution fluorescence imaging was required for imaging of ChAT/vAChT and eGFP co-labelling in synaptic endbulbs. Data were acquired as single scan images or z-stack images, with multiple scans capturing a thickness of 3-7 µm of tissue at z-scanning intervals of 0.4-0.6 µm. Figures were compiled from these images using Canvas Graphics software (ACD Systems International Inc., Victoria, Canada).

Quantitative approaches

To document the relative proportion of MNs in DLN and DMN that were eGFP$^+$ in male (n = 5) and female (n = 5) Cx36^{BAC}::eGFP mice, consecutive horizontal spinal cord sections containing the entirety of these motor nuclei were taken for immunostaining for ChAT or both ChAT and vAChT in one fluorescent channel, together with labelling for eGFP in the green fluorescent channel. In each motor nucleus, once MNs were identified by virtue of their labelling with cholinergic markers, the same sections were then analyzed for determination of those MNs that were eGFP$^+$. To avoid including in adjacent sections the same MNs more than once, cells were tallied only when they exhibited a clear nucleus, which indicated for that section that the tissue had been sectioned close to the center of the cell being considered for inclusion. For samples from male mice, counts were separately taken from the left- or the right-hand side of each spinal cord section. From the total number of eGFP$^+$ and ChAT$^+$ MNs for each animal, the percentage of MNs in the DLN or DMN that were eGFP$^+$ for each side, for each individual animal was calculated. In female mice, which had fewer eGFP$^+$ cells, the counts were instead pooled for the left- and right-hand sides together and then percentages calculated. Some slides were used to determine the percentage of MNs in the DLN and DMN of male (n = 5) Cx36^{BAC}::eGFP mice that were both eGFP$^+$ and Cx36$^+$. To accomplish this, counts were conducted as above in adjacent horizontal spinal cord sections that were simultaneously labelled with ChAT or both ChAT/vAChT in one fluorescent channel, for eGFP in the second channel and for Cx36 in the third channel.

To determine the relative innervation of target bulbocavernosus, external anal sphinter, ischiocavernosus and external urethral sphincter muscles by the eGFP$^+$ and eGFP$^-$ MN subpopulations of DLN and DMN, we conducted counts of synaptic endbulbs in these muscles, which were identified by their immunofluorescence for vAChT/ChAT$^+$, and then determined the proportion of these that were eGFP$^+$. vAChT/ChAT$^+$ positive synaptic endbulbs were analyzed in 20 image fields of each muscle, which were taken from 5 adult male Cx36^{BAC}::eGFP mice, and from counts of those that were eGFP$^+$ the percentage of synaptic endbulbs that were eGFP$^+$/field was calculated. The data for all analyses was compiled in Microsoft Excel software, with descriptive statistics and comparisons performed using GraphPad Prism software (San Diego, CA, USA), Version 10.1.2 (234).

Results

eGFP expression in MNs of DLN and DMN in Cx36^{BAC}::eGFP mice

In our earlier report on Cx36 localization in MNs of DLN and DMN in mice and rats as well as eGFP expression in these MNs of transgenic Cx36^{BAC}::eGFP mice, where eGFP expression is driven by the Cx36 promoter, our qualitative observations indicated that eGFP was robustly expressed in only a subpopulation of MNs in each of these motor nuclei and only weakly or not at all in an additional subset [32]. At the time, we had reason for concern that eGFP reporter expression in these mice may not fully reveal neurons that express eGFP due to incomplete BAC transgene integration, which is

known to occur [58]. Indeed, we have found brain regions in which neurons are known to express Cx36, but which lack eGFP expression in the $Cx36^{BAC}$::eGFP mice line [52]. Further, we have noted a progressive reduction in the fidelity of eGFP expression in these mice due to excessive inbreeding, which causes reduced $Cx36^{BAC}$ transmission, according to cautionary notes provided by the supplier of these mice. Since then, we have undertaken routine backcrossing of these transgenic mice with wild-type mice, which has resulted in robust eGFP expression in electrically coupled neurons known to express Cx36, including retrieval of eGFP production in some, though not all, neurons previously showing false-negative expression of this reporter.

In the $Cx36^{BAC}$::eGFP mice, we re-examined expression of eGFP in MNs of sexually dimorphic DLN and DLM in lower lumbar regions of male and female mice. As an immunofluorescence marker for MNs, we interchangeably used either the traditional marker ChAT with simultaneous labelling for vAChT, which in combination was found to produce more reliable visualization of MNs, or alternatively, we used immunolabelling for peripherin. Peripherin is an intermediate filament protein highly expressed in neurons of the peripheral nervous system but is also found in central neurons that have projections to peripheral structures such as sympathetic preganglionic neurons (SPNs) and MNs, as well as in peripheral neurons that have projections to the CNS such as primary afferent neurons in dorsal root ganglia and their centrally projecting fibers in the spinal cord [59-61]. Sexually dimorphic motor nuclei at lower lumbar levels were identified, in part, according to the spinal cord atlas of Watson *et al*. [62], as well as from descriptions of MNs in these nuclei retrogradely labelled from the pudendal nerve or their target muscles [38, 40]. In horizontal sections of L5-S2 spinal cord segments of adult male $Cx36^{BAC}$::eGFP mice, the DLN located in the ventrolateral quadrant of the ventral horn was readily identified by additional features, including the unusually tight intermittent clustering of its constituent ChAT/$vAChT^+$ motoneuronal somata [40, 63], and by the prominent bundling of dendrites arising from those somata (**Figure 1A**). Within DLN, randomly distributed $eGFP^+$ MNs were seen intermingled among ChAT/$vAChT^+$ MNs that were $eGFP^-$ (**Figure 1A**).

The MNs in DMN in horizontal sections of L5-L6 spinal cord segments of adult male $Cx36^{BAC}$::eGFP mice (**Figure 1B**) were equally identifiable by their characteristic distribution on either side of the midline, and localization beneath and/or adjacent to the central canal medially and at the apex and/or flanking the ventral funiculus more ventrally, as well as by their more dispersed appearance compared with those in the DLN and their dendritic projections across the midline [64-66]. As in DLN, $eGFP^+$ MNs in DMN were seen distributed among ChAT/$vAChT^+$ MNs that were $eGFP^-$ (**Figure 1B**). The $eGFP^+$ vs. $eGFP^-$ MNs in either DLM or DMN displayed no recognizable qualitative morphological features, such as somal size or dendritic arborizations, that would distinguish these two subpopulations.

The DLN and DMN are termed sexually dimorphic because the development and maintenance of their constituent MNs in males is dependent on adequate levels of circulating androgens, and because these neurons in females vs. males are far fewer and smaller in size [34, 35, 67-69]. As in male mice, our examination of labelling for eGFP in the DLN of $Cx36^{BAC}$::eGFP female mice revealed subpopulations of tightly clustered ChAT/$vAChT^+$ MNs that were either $eGFP^+$ or $eGFP^-$ (**Figure 2A**). In contrast, far fewer MNs in the DMN of female $Cx36^{BAC}$::eGFP mice were seen to express eGFP or expressed this reporter weakly when compared to expression levels seen in males (**Figure 2B**, **2C**). Results from quantitative analyses of the proportions of MNs in DMN and DLN of male and female $Cx36^{BAC}$::eGFP mice are shown graphically in **Figure 3**. In males, the percentage of $peripherin^+$ MNs that were $eGFP^+$ was quantified in DMN and DLN separately on the left and right sides of the cord showed good correspondence between these sides, yielding mean ± s.e.m. values of 54.5 ± 6.6% and 55.4 ± 2% $eGFP^+$ MNs in the DMN and DLN respectively when counts from the two sides were pooled. In females, analyses of MNs in the left- and right-hand sides pooled together gave mean ± s.e.m. values for ChAT/$vAChT^+$ MNs that were $eGFP^+$ in DMN and DLN of 9 ± 3% and 28 ± 5% respectively. One way ANOVA with Dunnet's post hoc test indicated that, in addition to other sexually dimorphic features these neurons exhibit, they show differential eGFP reporter expression in $Cx36^{BAC}$::eGFP mice, with

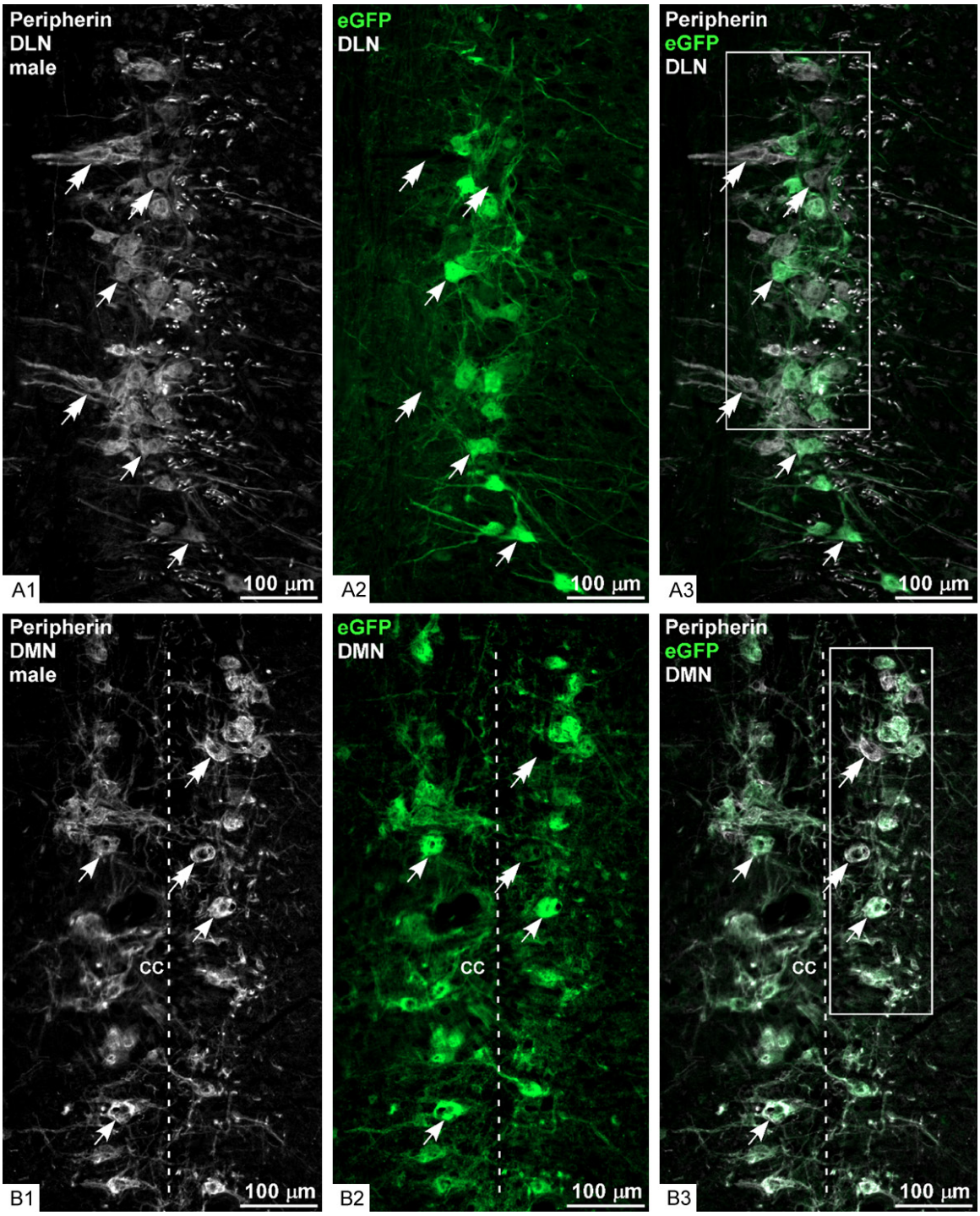

Figure 1. Immunofluorescence labelling of eGFP reporter in subpopulations of MNs in sexually dimorphic motor nuclei of adult male $Cx36^{BAC}$::eGFP mice. (A) Lower lumbar horizontal spinal cord section labelled for the MN marker peripherin (A1) and Cx36 expression reporter eGFP (A2) showing a column of MN in the DLN wherein a portion of peripherin$^+$ MNs (A1, arrows) are eGFP$^+$ (A2, arrows), while a separate sub portion is devoid of labelling for eGFP (A1, A2, double arrows), as evident in image overlay (A3, arrows, double arrows). (B) Double labelled horizontal section of lower lumbar spinal cord with medially located columns of sexually dimorphic MNs in DMN, shown bilaterally, double labelled for peripherin (B1) and eGFP (B2). Intermittent clusters of peripherin$^+$ MNs on either side of the central canal (cc, dotted line) contain MNs that are both peripherin$^+$ and eGFP$^+$ (B1, B2, arrows), while some MNs in these clusters lack labelling of eGFP (B1, B2, double arrows), as shown in image overlay (B3).

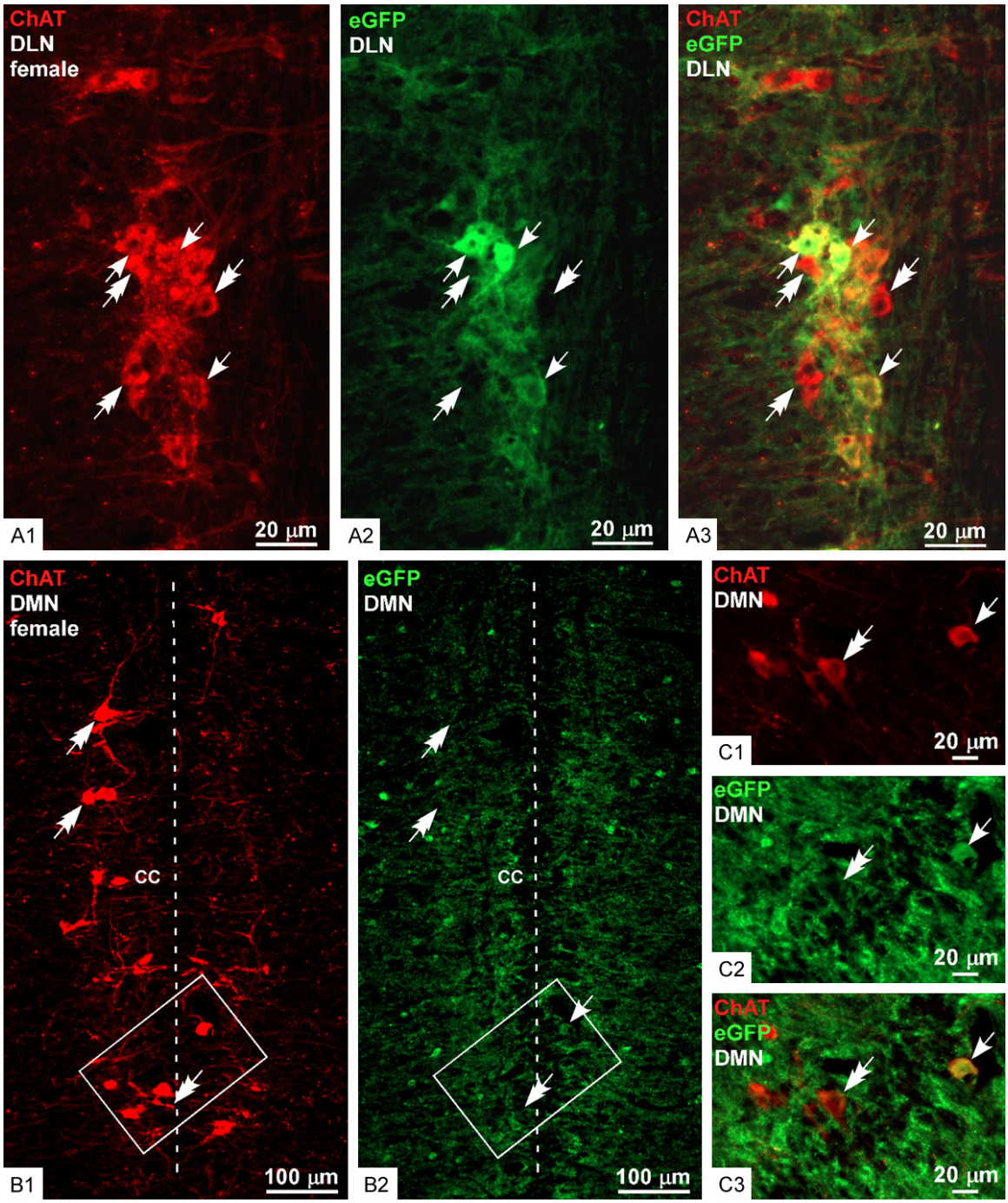

Figure 2. Immunofluorescence labelling of eGFP reporter in subpopulations of MNs in sexually dimorphic motor nuclei in lower lumbar horizontal spinal cord sections of adult female Cx36^{BAC}::eGFP mice. (A) Image of DLN in a double labelled section showing ChAT$^+$ MNs (A1, arrows and double arrows) that are either eGFP$^+$ (A1, A2, arrows) or eGFP$^-$ (A1, A2, double arrows), as seen in image overlay (A3, arrows, double arrows). (B) Image of DMN in a double labelled section showing ChAT$^+$ MNs bilaterally (B1, double arrows) (cc, central canal, dotted line) that are largely eGFP$^-$ (B1, B2, double arrows). (C) Magnification of the boxed area in (B), showing several ChAT$^+$ MNs (C1, arrow and double arrow), where most are eGFP$^-$ (C2, double arrow) and one is weakly labelled for eGFP (C2, arrow) as seen in overlay image (C3, arrow).

significantly greater eGFP$^+$ MNs in male mice *vs.* female mice for both the DMN (P = 0.002) and the DLN (P = 0.011). This result suggests that the eGFP$^+$ MNs may correspond to the sex-

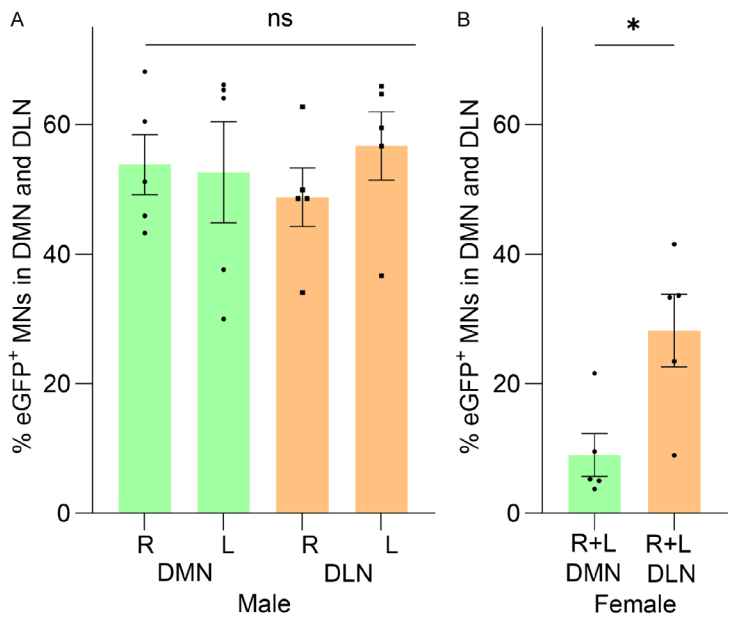

Figure 3. Histograms summarizing the proportions of visualized and counted ChAT$^+$ MNs in sexually dimorphic DMN and DLN that were eGFP$^+$ in adult male and female Cx36^{BAC}::eGFP mice. A. The total ChAT$^+$/vAChT$^+$ MNs/field was counted and the percentage of those that were eGFP$^+$ was calculated separately from the right (R) and left (L) DMN and DLN of five adult male Cx36^{BAC}::eGFP male mice. Average percentages of ChAT/vAChT$^+$/eGFP$^+$ MNs for each side from individual mice are represented by a dot. Error bars represent percentage mean ± s.e.m. for the R (53.8 ± 4.6%) and L (52.6 ± 7.8%) sides of the DMN and the R (48.8 ± 4.5%) and L (56.7 ± 5.6%) sides of the DLN. ANOVA indicated that the proportion of MNs in the DLN and DMN that expressed eGFP did not significantly differ between the two sides for each nucleus or between the two motor nuclei. B. Similar analyses were undertaken in female Cx36^{BAC}::eGFP mice, where data from the left and right sides of the spinal cord were pooled for each nucleus. The percentage mean ± s.e.m. was (9.1 ± 3.3%) and (28.2 ± 5.6%) for the DMN and DLN, respectively. Two tailed Student's t test analysis of this data for female mice indicated a significantly lower percentage of eGFP expression in MNs of DMN vs. DLN. For comparison of data from male and female mice, data from the right and left sides for males were separately pooled for the DMN and DLN and analyzed *vs.* data from the DMN and DLN of female mice (not shown) by Brown-Forsyth and Welch's one way ANOVA with Dunnet's T3 post-hoc test, revealing a significantly lower percentage of MNs with eGFP expression in both the DMN ($P = 0.0016$) and DLN ($P = 0.011$) of female *vs.* male mice. Error bars represent percentage mean ± s.e.m., * indicates $P = 0.019$, ns indicates not significant.

ually dimorphic population in these nuclei vs. the eGFP$^-$ non-sexually dimorphic population, as discussed below.

Target muscles innervated by eGFP$^+$ vs. eGFP$^-$ MNs in DLN and DMN

Sexually dimorphic MNs in the lower lumbar spinal cord innervate striated muscles located in the pelvic floor. As depicted in **Figure 4**, MNs in DLN innervate the ischiocavernosus muscle and the external urethral sphincter, while those in the DMN innervate the bulbocavernosus muscle and the external anal sphincter [38, 40]. In both the DMN and DLN, MNs projecting to sphincter muscles are considered to be sexually non-dimorphic [41, 70] and are completely intermingled with, and are difficult to distinguish from, sexually dimorphic MNs innervating bulbocavernosus and ischiocavernosus muscles, respectively, in the absence of retrograde labelling from those target muscles [38, 64]. Here, we sought to determine the peripheral target muscles of eGFP$^+$ vs. eGFP$^-$ MNs in the sexually dimorphic nuclei by examining Cx36^{BAC}::eGFP mice for eGFP localization in synaptic end bulbs at motor endplates in the target muscles of these nuclei. Immunofluorescence labelling of ChAT/vAChT as a maker for end bulbs was robustly visualized in each of those muscles, including the bulbocavernosus muscle (**Figure 5A**), external anal sphincter muscle (**Figure 5B**), the ischiocavernosus muscle (**Figure 5C**) and external urethral sphincter muscle (**Figure 5D**). Fortuitously, labelling of eGFP was equally prominent in, for example, the ischiocavernosus muscle such that eGFP in axons contained in fiber bundles could be seen co-localized with labelling for ChAT/vAChT in these bundles (**Figure 5E**), and individual fibers double labelled for ChAT/vAChT and eGFP could be followed to their synaptic end bulbs at end-plates (**Figure 5F**) that also displayed a high degree of cholinergic marker co-localization with eGFP (**Figure 5G**). Numerous ChAT/vAChT$^+$ synaptic end bulbs viewed either edge on or en face were found to be eGFP$^+$ in both the ischiocavernosus (**Figure 6A**, **6B**) muscle and bulbocavernosus muscle (**Figure 6C**, **6D**). In contrast, very few ChAT/vAChT$^+$ synaptic end bulbs displayed labelling for eGFP in the external urethral sphincter muscle (**Figure 6E**) or the external anal sphincter

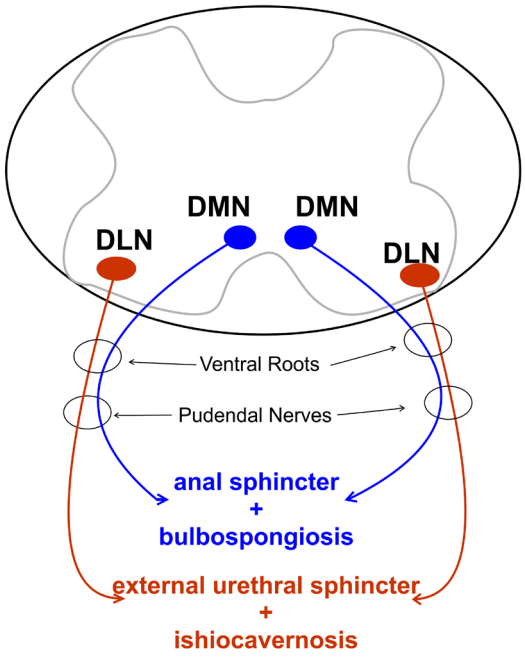

Figure 4. Diagram showing the locations of the DLN and the DMN in the lower lumbar region of the spinal cord and the peripheral projections of their MNs to sexually dimorphic perineal muscles (ischiocavernosis and bulbocavernosus, aka bulbospongiosis muscles) and to non-sexually dimorphic muscles (external anal sphincter and external urethral sphincter).

muscle (**Figure 6F**). Images like those shown in **Figure 6** were used for quantitative analyses of the percentage of ChAT/vAChT^{+} synaptic end bulbs that displayed labelling for eGFP in each of the aforementioned muscles in Cx36^{BAC}::eGFP mice. For quantitative analyses, twenty fields from each muscle type were taken for counts of total ChAT/vAChT^{+} synaptic end bulbs/field and those that were eGFP^{+}/field, with results presented in **Table 2** and **Figure 7**, where 97 ± 1.6% and 95 ± 1.3% of synaptic end bulbs in the ischiocavernosus and bulbocavernosus muscles, respectively, were found to be eGFP^{+}, while 1.7 ± 0.8% and 1.1 ± 0.6% of those in the external anal and external urethral sphincter muscles, respectively, were eGFP^{+}. These results indicate differential projections of eGFP^{+} vs. eGFP^{-} MNs in sexually dimorphic motor nuclei to their target muscles, with the eGFP^{+} population selectively innervating the sexually dimorphic ischiocavernosus and bulbocavernosus muscles.

Target muscles innervated by eGFP^{+} vs. eGFP^{-} MNs in the cremaster motor nucleus

We recently reported heterogeneous expression of eGFP in MNs of the upper lumbar (i.e., L1-L2) sexually dimorphic cremaster motor nucleus of male and female Cx36^{BAC}::eGFP mice, where a little over 60% and a little under 50% of MNs in this nucleus expressed eGFP, respectively [33]. Like the lower lumbar sexually dimorphic MNs, cremaster MNs are designated sexually dimorphic based on their greater numbers, larger size and differential innervation density by serotonergic and peptidergic fibers in males vs. female animals, and on the absence of cremaster muscles in females [36, 37, 39, 71, 72], where those MNs are thought instead to innervate ligaments of the uterus [36]. Although cremaster MNs innervate a single cremaster muscle, different portions of this muscle are morphologically distinct and either envelop the testes or surround the spermatic cord [49], where differential activity in these separate portions may serve different physiological outcomes. Here, we took advantage of the robust anterograde transport of eGFP in MNs to their peripheral synaptic end bulbs in Cx36^{BAC}::eGFP mice to examine the possibility of differential projections of eGFP^{+} vs. eGFP^{-} cremaster MNs to their possibly segregated innervation of cremaster muscle enveloping the testes (cremaster-t) vs. that surrounding the spermatic cord (cremaster-sc). As in sexually dimorphic muscles innervated by DMN and DML, cremaster-t muscle containing ChAT/vAChT^{+} synaptic end bulbs were heavily labelled for eGFP in Cx36^{BAC}::eGFP mice (**Figure 8A**), and occasionally eGFP^{+} axons could be followed to those end bulbs (**Figure 8B**). Cremaster-sc muscle lying adjacent to the spermatic cord also contained a rich investment of ChAT/vAChT^{+} synaptic end bulbs (**Figure 8C**). However, the ChAT/vAChT^{+} synaptic end bulbs in cremaster-sc muscle were entirely devoid of labelling for eGFP (**Figure 8D**). This was especially evident in sections containing both cremaster-t muscle that displayed ChAT/vAChT^{+}/eGFP^{+} end bulbs and that was separated from cremaster-sc by a lamina tissue presumed to be the spermatic facia next to the spermatic cord [57], where ChAT/vAChT^{+} synaptic end bulbs were devoid of labelling for eGFP (**Figure 8E**).

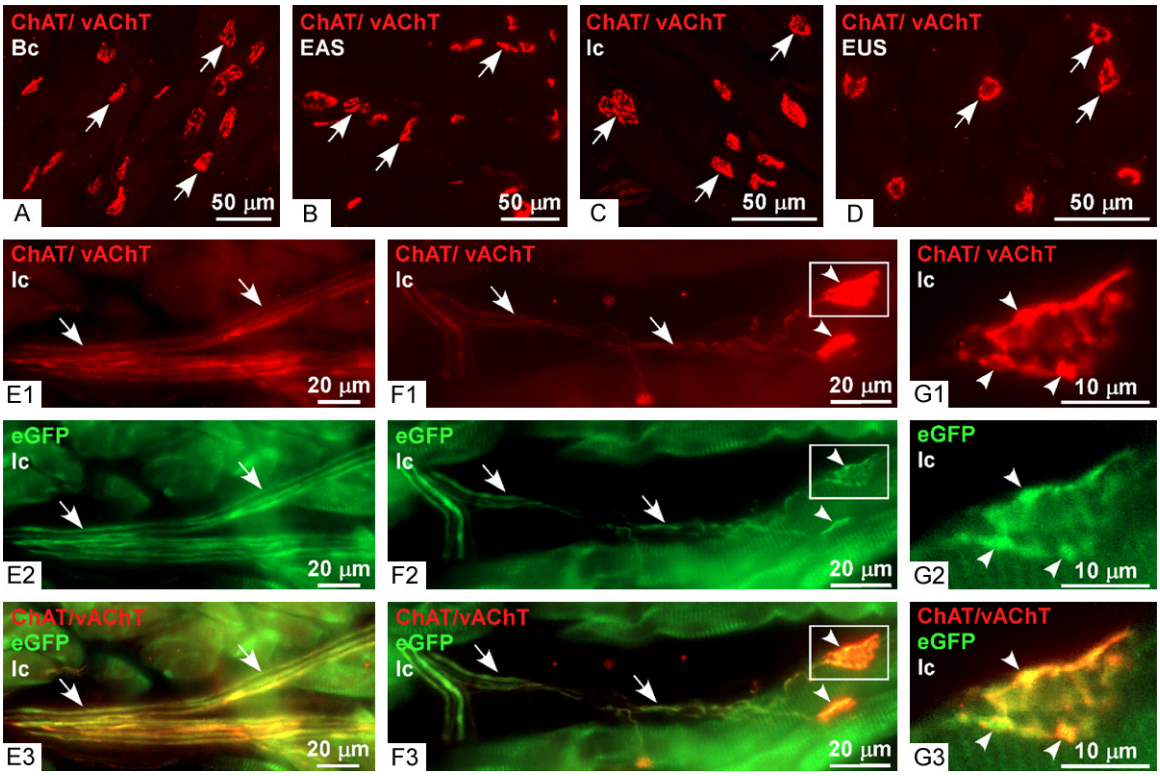

Figure 5. Immunofluorescence labelling of ChAT/vAChT and eGFP in muscles innervated by MNs in sexually dimorphic DMN and DLN in adult male Cx36^{BAC}::eGFP mice. (A-D) Appearance of ChAT/vAChT^{+} synaptic end bulbs (arrows) at motor endplates in the two muscle groups innervated by DMN: Bc, bulbocavernosus (A); EAS, external anal sphincter (B); and two innervated by DLN: Ic, ischiocavernosis (C); and EUS, external urethral sphincter (D). (E) Double immunofluorescence labelling in a field of the ischiocavernosis muscle showing bundles of ChAT/vAChT^{+} fibers (E1, arrows) that are also robustly labelled for eGFP (E2, arrows), with co-localization of labelling seen in image overlay (E3, arrows). (F) Double labelling in the ischiocavernosis muscle showing ChAT/vAChT^{+} motor axons (F1, arrows) that are also eGFP^{+} (F2, arrows) and that can be followed to synaptic end blubs intensely labelled for ChAT/vAChT (F1, arrowheads) co-localized with eGFP (F2, F3, arrowheads) at motor endplates. (G) Magnification of boxed area in (F) showing dispersed labelling of both ChAT/vAChT (G1, arrowheads) and eGFP (G2, arrowheads) within a synaptic end bulb reflecting its convoluted nature, and co-localization of this dispersed labelling (G3, arrowheads).

Immunofluorescence labelling of Cx36 and ChAT in Cx36^{BAC}::eGFP mice

We have previously reported on the characteristics of immunofluorescence labelling of Cx36 in the DLN and DMN of mice and rats. As in other regions of the CNS we have examined [2, 11, 32, 51, 56, 73-75], immunofluorescence labelling of Cx36 has an exclusively punctate appearance (*i.e.,* Cx36-puncta) among MNs in the sexually dimorphic motor nuclei (**Figure 9**) and is invariably localized to the surface of neuronal elements. Intracellular labelling of Cx36 appears undetectable at least *in vivo*, perhaps due to masking of Cx36 epitopes at intracellular compartments that precludes binding of antibodies. This localization of immunolabelling at Cx36-puncta is well correlated with sites of ultrastructurally-defined Cx36-containing neuronal gap junctions [76-82], thus allowing those puncta to serve as markers for such junctions *in vivo.*

Here, we sought to determine the degree to which Cx36-puncta might be restricted to MNs in which the presence of eGFP served as a reporter for Cx36 expression. Using Cx36BAC::eGFP mice, we examined the localization of immunofluorescent Cx36-puncta in horizontal spinal cord sections through the dorsal to ventral extent of the DLN and DMN, where the sections were simultaneously immunolabelled for both eGFP and the MN marker ChAT. As expected, and as shown by low magnification overview of the DLN in **Figure 9A**, Cx36-puncta were often seen localized to ChAT^{+} MN

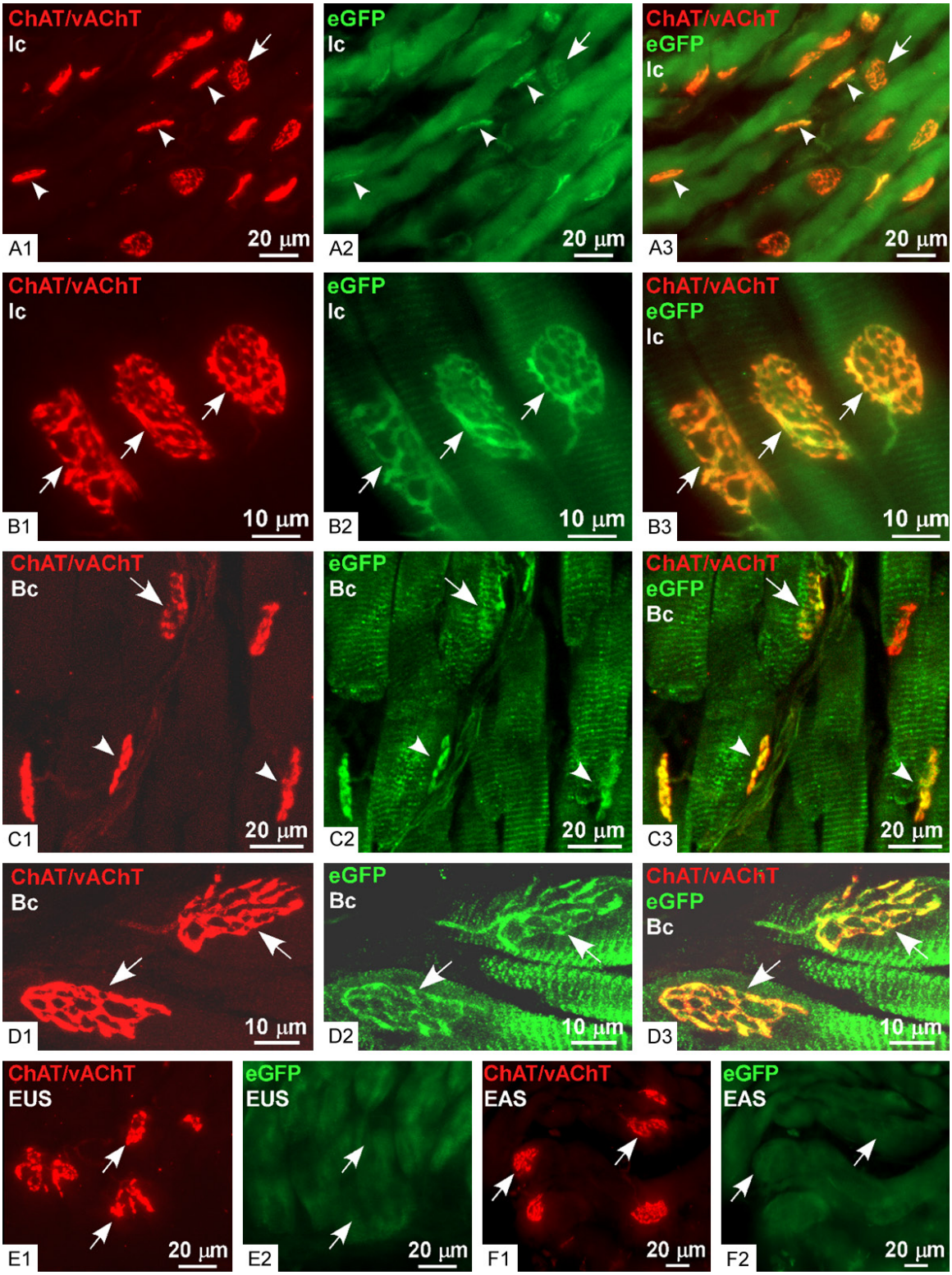

Figure 6. Target muscle innervation by eGFP$^+$ vs. eGFP$^-$ MNs in sexually dimorphic DLN and DMN of adult male Cx36^{BAC}::eGFP mice. Images shown are examples of fields double labelled for ChAT/vAChT and eGFP and used for quantification of the proportion of ChAT/vAChT$^+$ synaptic end bulbs at motor endplates that were eGFP$^+$ in each of the four muscles groups innervated by DLN and DMN. (A) Ischiocavernosis muscle showing numerous ChAT/vAChT$^+$ synaptic end bulbs (A1) that are also eGFP$^+$ (A2, A3), where some end bulbs are seen in edge on view (arrowheads) and others in *en face* view (arrows). (B) Higher magnification confocal images showing the appearance of three synaptic end blubs at motor endplates in the ischiocavernosis muscle, with near exact correspondence of labelling for

ChAT/vAChT (B1, arrow) and eGFP (B2, arrows), as seen in image overlay (B3, arrows). (C) Bulbocavernosus muscle showing edge on (arrowheads) and en face (arrow) views of synaptic end bulbs at motor endplates double labelled for ChAT/vAChT (C1) and eGFP (C2), with co-localization of labelling evident in image overlay (C3). (D) Higher magnification confocal images of synaptic end bulbs in bulbocavernosus muscle labelled for ChAT/vAChT (D1, arrows) and eGFP (D2, arrows), and co-localization of labelling (D3) in these bulbs. (E, F) external urethral sphincter, EUS, muscle (E) and external anal sphincter, EAS, muscle (F) double labelled for ChAT/vAChT (E1, F1) and eGFP (E2, F2) showing ChAT/vAChT$^+$ synaptic end bulbs at motor end-plates (E, F, arrows) that are devoid of labelling for eGFP (E2, F2, arrows).

Table 2. Total ChAT/vAChT$^+$ synaptic end bulbs per image field, the number of those that were eGFP$^+$ or eGFP$^-$ and the average percentage of endplates that were eGFP$^+$ per field

Muscle	Total endplates counted in twenty fields	Average endplates per field	Endplates		Average % eGFP$^+$ endplates per field*
			eGFP$^-$	eGFP$^+$	
Bulbospongiosis	233	11.7	7	226	96.9 ± 1.6
External anal sphincter	258	12.9	254	4	1.7 ± 0.8
Ischiocavernosis	286	14.3	16	270	94.4 ± 1.3
External uretheral sphincter	266	13.3	263	3	1.1 ± 0.6
Cremaster	227	11.35	17	210	93.1 ± 0.02

Data was collected from twenty image fields per muscle in sections of the bulbospongiosis, external anal sphincter, ischiocavernosis, external urethral sphincter and cremaster muscles taken from five male Cx36^{BAC}::eGFP mice. *Data is expressed as mean % ± s.e.m.

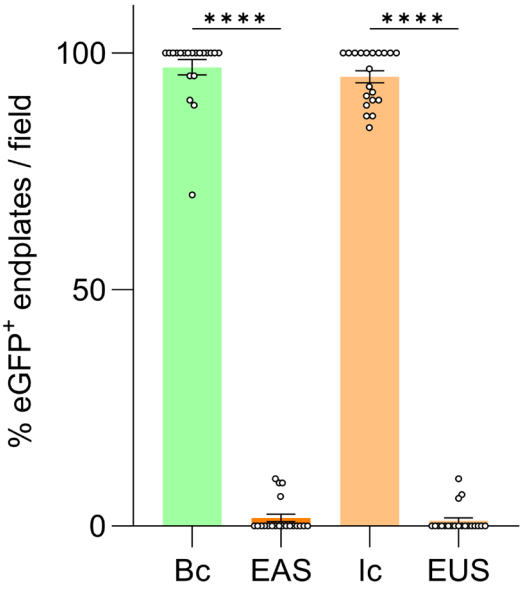

Figure 7. Histogram displaying percentage of ChAT/vAChT$^+$ synaptic end bulbs at motor endplates that were eGFP$^+$ in the bulbocavernosus muscle (Bc) and anal sphincter (EAS) innervated by DMN, and percentage of ChAT/vAChT$^+$ end bulbs that were eGFP$^+$ in the ischiocavernosis muscle (Ic) and external urethral sphincter (EUS) innervated by DLN. Each dot represents an image of a muscle field in which the percentage of ChAT/vAChT$^+$ synaptic end bulbs that were eGFP$^+$ was examined. Analysis by Brown-Forsyth and Welch's one-way ANOVA with Dunnet's T3 post-hoc test indicated that both Bc and Ic muscles had a significantly greater number of eGFP$^+$ end bulbs compared with both the EAS and the EUS muscles. Error bars represent percentage mean ± s.e.m., **** indicates $P < 0.0001$.

somata and dendrites that were immunolabelled for eGFP. These puncta also frequently occurred at close appositions between eGFP$^+$ neuronal elements, including neuronal somata (**Figure 9B**). Unexpectedly however, Cx36-puncta in the DLN were also widely distributed among ChAT$^+$ MNs that were unlabelled for eGFP (**Figure 9A** and **9B**). Further, dense clusters of Cx36-puncta were often observed at close appositions between ChAT$^+$ MNs where one of the apposing cells was labelled for eGFP and the other was not (**Figure 9A** and **9C**). Similar results were obtained in the DMN, where Cx36-puncta commonly occurred at sites of apposition between eGFP$^+$ neuronal elements, such as dendro-somatic (**Figure 9D**) and dendro-dendritic (**Figure 9E**) appositions. In addition, Cx36-puncta were localized along eGFP$^+$ dendrites at sites that were in close proximity to eGFP$^-$ MN somata labelled for ChAT (**Figure 9F**) as well as at close appositions between eGFP$^+$ and eGFP$^-$ MNs (**Figure 9G**). Some eGFP$^-$ MN somata had striking clusters of Cx36-puncta associated with their somata (**Figure 9H**), similar to that we earlier described in DLN and DMN in rat [32], and such clusters of puncta were found localized to close appositions between MN, including those devoid of immunolabelling for eGFP (**Figure 9I**).

In images of both DLN and DMN with MNs labelled for ChAT such as those shown in **Figure 9**, we quantitatively examined the percentage

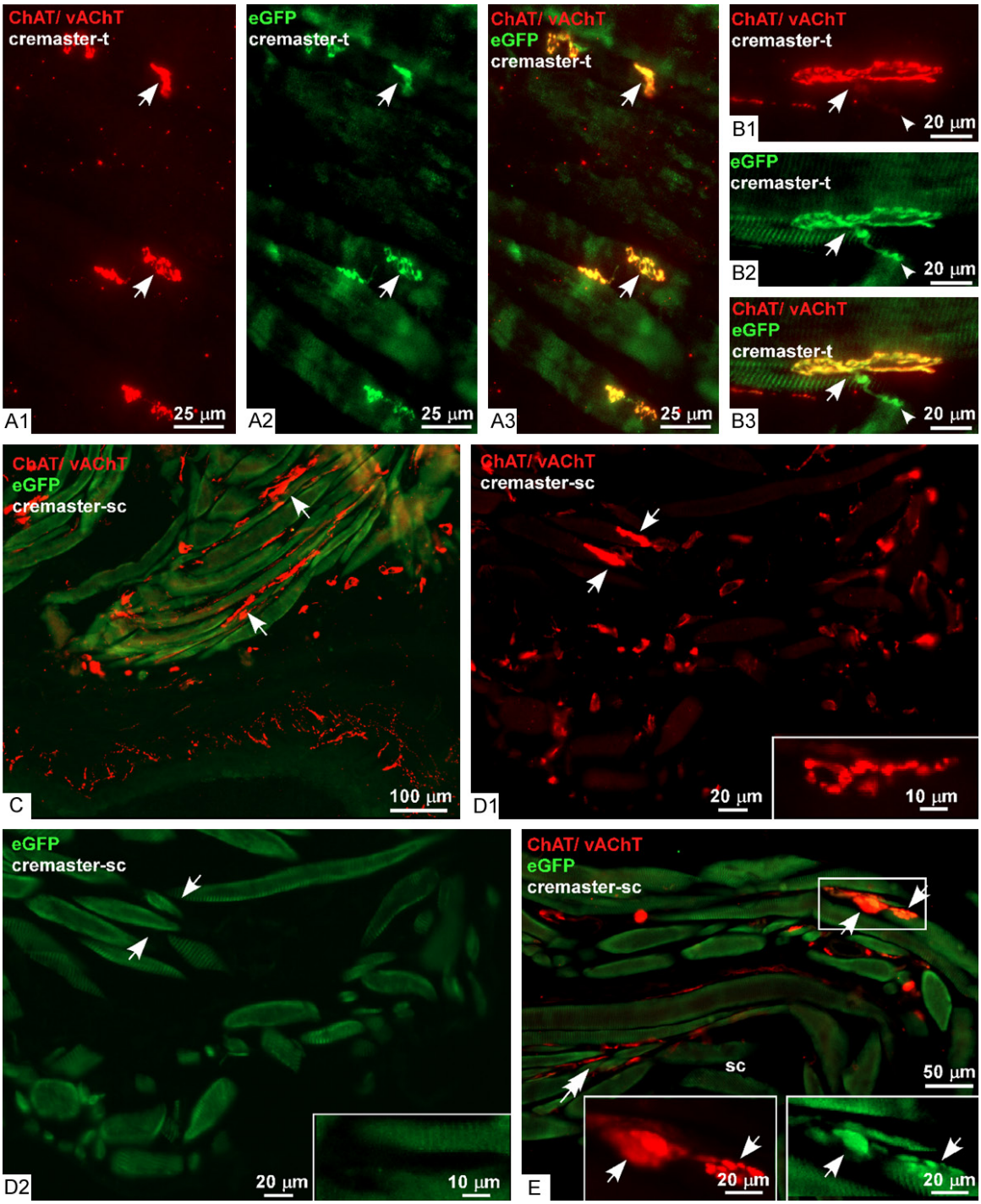

Figure 8. Double immunofluorescence labelling of cremaster muscle surrounding testes (cremaster-t) and spermatic cord (cremaster-sc) innervated by upper lumbar sexually dimorphic cremaster MNs in adult male Cx36^{BAC}::eGFP mice. (A) Images of ChAT/vAChT^{+} synaptic end bulbs (A1, arrows) at motor end plates that are also labelled for eGFP (A2, arrows) in cremaster muscle surrounding testes, with co-localization shown in image overlay (A3, arrows). (B) Higher magnification showing labelling of ChAT/vAChT (B1, arrow), eGFP (B2, arrow) and their co-localization (B3, arrow) at a synaptic end bulb in cremaster muscle surrounding testes, and an axon weakly labelled for ChAT/vAChT, but robustly labelled for eGFP converging on the end bulb (arrowhead). (C) Low magnification showing cremaster muscle associated with and in close proximity to the spermatic cord (sc), in a section labelled for ChAT/vAChT localized to numerous synaptic end bulbs at motor end plates (arrows). (D) Higher magnification image showing ChAT/vAChT^{+} synaptic end bulbs at motor endplates (D1, arrows) in cremaster muscle surrounding spermatic cord, where end bulbs are devoid of labelling for eGFP (D2, arrows), with the inset showing a magnified single ChAT/vAChT^{+}/

eGFP$^-$ end bulb. (E) Double labelling of ChAT/vAChT and eGFP in cremaster muscle surrounding spermatic cord where ChAT/vAChT$^+$ synaptic end bulbs are eGFP$^-$ (double arrow), and outside of which separated by a laminar sheath (spermatic fascia, arrowheads) lies cremaster muscle associated with testes where ChAT/vAChT$^+$ synaptic end bulbs display robust labelling for eGFP (arrows), as seen in the boxed area magnified in the inset showing end bulbs labelled for both ChAT/vAChT and eGFP (arrows).

of eGFP$^+$ and eGFP$^-$ MNs that were decorated with Cx36-puncta around their somata and/or initial dendrites where these could be followed back to their somata of origin. Among 381 MNs examined in the DLN, which included 207 that were eGFP$^+$, 98 ± 0.8% of all MNs and 99 ± 0.9% of those MNs that were eGFP$^+$ harbored Cx36-puncta. Among 385 MNs in the DMN, of which 192 were eGFP$^+$, Cx36-puncta were associated with 93 ± 1.4% of the total MN population and with 95 ± 1.4% of the eGFP$^+$ subpopulation.

Discussion

Our results demonstrate the presence of roughly equal numbers of eGFP$^+$ and eGFP$^-$ MNs in lower lumbar sexually dimorphic nuclei of adult male Cx36^{BAC}::eGFP mice, and a much lower percentage of eGFP$^+$ MNs in these nuclei of female Cx36^{BAC}::eGFP mice. Further, we find in male mice that the eGFP$^+$ population of MNs in both the DMN and DLN project almost exclusively to sexually dimorphic bulbocavernosus and ischiocavernosus muscles, respectively, while the eGFP- MNs in the DMN and DLN project preponderantly to the sexually non-dimorphic external anal sphincter and external urethral sphincter, respectively. Our finding that eGFP$^+$ MNs in the DMN and DLN project to sexually dimorphic peripheral muscles in male mice, which are absent in female mice, is consistent with the far fewer eGFP$^+$ MNs in these nuclei of female mice. Similarly, we found differential projection patterns of MNs displaying what we previously reported to be heterogeneous eGFP reporter for Cx36 expression in the cremaster motor nucleus [33], such that MNs representing slightly greater than 60% of the population in this nucleus that were eGFP$^+$ project to cremaster muscle surrounding the testes, while the remaining eGFP$^-$ MNs project to a portion of the same muscle, but which is associated with an anatomically separate region, namely the spermatic cord. Based on these results, together with the high correspondence between eGFP reporter expression in distinct neuronal populations of Cx36^{BAC}::eGFP mice with those same neurons known to be e-coupled [2, 22, 50, 83], it might be considered that sexually dimorphic motor nuclei contain both e-coupled and non-coupled MNs. This possibility, however, is excluded by our quantitative analysis of Cx36 expression in the DLN and DMN of Cx36^{BAC}::eGFP mice, where we found Cx36-puncta associated with nearly all MNs, suggesting that the vast majority of these MNs have e-coupling capability. We previously found Cx36-puncta associated with similarly high percentages of MNs in the DLN and DMN of rats and wild-type C57BL/6 mice [32]. This is consistent with observations of gap junctions linking these MNs and electrophysiological evidence for their e-coupling [30, 31, 84]. Thus, it appears that lack of eGFP in a subset of MNs in DLN and DMN represents false-negative reporter expression despite our efforts to optimize breeding protocols to achieve robust eGFP expression in the Cx36^{BAC}::eGFP mice.

The sexually dimorphic DLN and DMN are unusual in that they are known to receive very little if any excitatory primary afferent innervation [38, 85, 86], which is reflected by a paucity of sensory afferent nerve terminals containing vesicular glutamate transporter-1 (vglut1) contacting MNs in these nuclei, as we previously reported [32]. In contrast, nearly all other MNs along the spinal cord, including those in the cremaster nucleus, are richly innervated by glutamatergic vglut1-containing terminals that are principally of primary afferent origin [87]. We also previously reported that Cx36-puncta are localized at most if not all vglut1$^+$ terminals on MNs, forming what are termed mixed chemical/electrical synapses [74]. The absence of vglut1$^+$ terminals and their associated Cx36-puncta on MNs in DLN and DMN allowed our documentation of Cx36-puncta localized to gap junctions linking various combinations of eGFP$^+$ and eGFP$^-$ MNs. A similar analysis was not possible in the cremaster nucleus due to the confounding presence of Cx36-puncta at mixed synapses on cremaster MNs. Hence, it remains to be determined whether the eGFP$^-$ population of MNs in the cremaster nucleus are devoid of

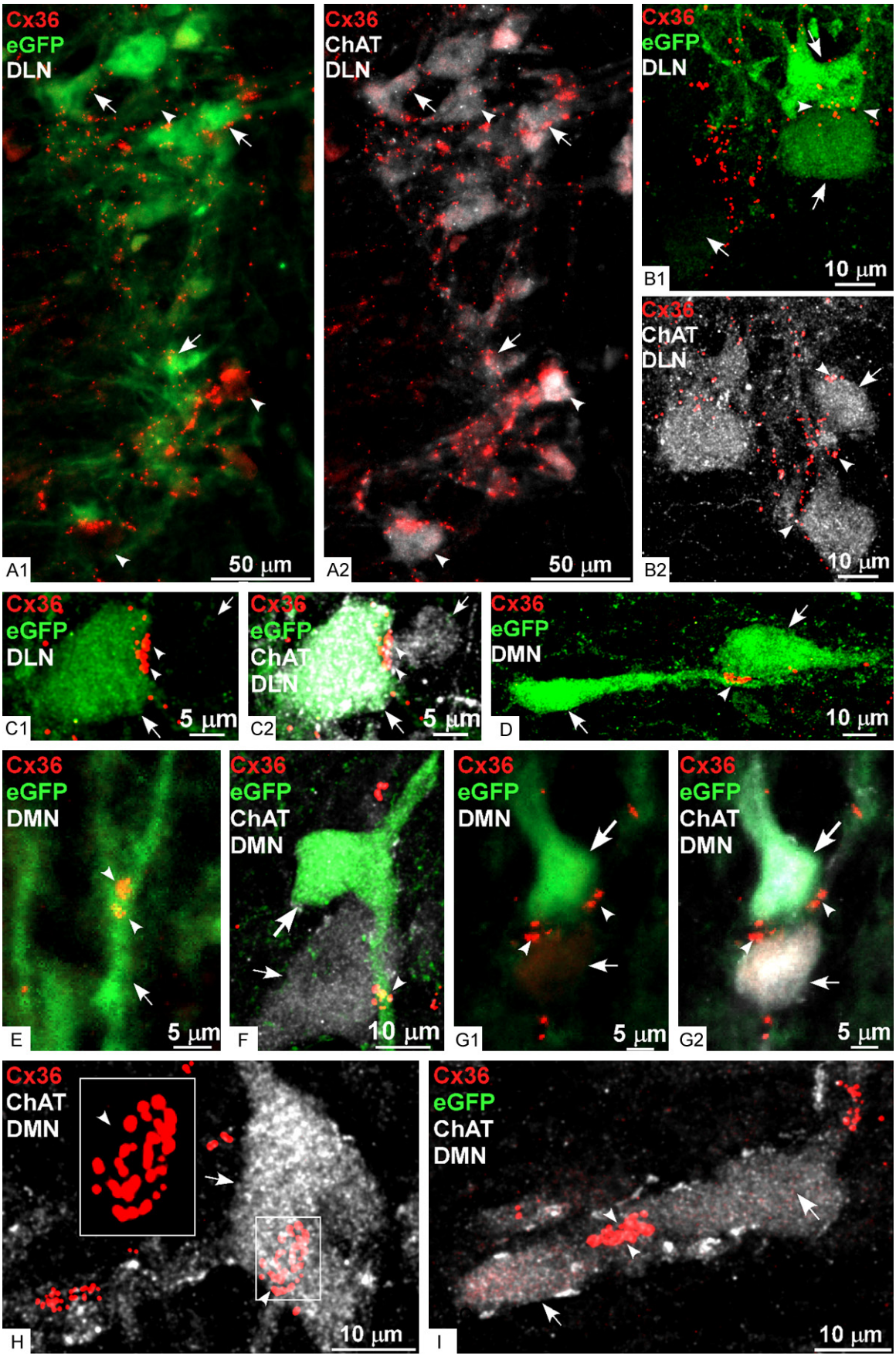
Cx36
eGFP
DLN
A1
50 μm
Cx36
ChAT
DLN
A2
50 μm
Cx36
eGFP
DLN
B1
10 μm
Cx36
ChAT
DLN
B2
10 μm
Cx36
eGFP
DLN
C1
5 μm
Cx36
eGFP
ChAT
DLN
C2
5 μm
Cx36
eGFP
DMN
D
10 μm
Cx36
eGFP
DMN
E
5 μm
Cx36
eGFP
ChAT
DMN
F
10 μm
Cx36
eGFP
DMN
G1
5 μm
Cx36
eGFP
ChAT
DMN
G2
5 μm
Cx36
ChAT
DMN
H
10 μm
Cx36
eGFP
ChAT
DMN
I
10 μm

Figure 9. Immunofluorescence localization of Cx36 in relation to immunolabelling for ChAT and eGFP among MNs in the DLN and DMN. (A) Low magnification overview of densely distributed Cx36-puncta associated with MNs that are both eGFP$^+$ and ChAT$^+$ (A1, A2, arrows) and with ChAT$^+$ MNs that are eGFP$^-$ (A1, A2, arrowheads) in the DLN. (B) Higher magnification of the DLN showing Cx36-puncta (B1, arrowheads) localized at close appositions of two eGFP$^+$ MNs (B1, arrows) and, in the same field, numerous Cx36-puncta (B2, arrowheads) among ChAT$^+$/eGFP$^-$ MNs (B2, arrows). (C) Image of an eGFP$^+$ MN (C1, large arrow) in DLN that is in close apposition with a portion of a ChAT$^+$/eGFP$^-$ MN (C1, C2, small arrow), showing a large cluster of Cx36-puncta at the site of apposition (C1, C2, arrowheads). (D, E) Images of eGFP$^+$ MNs (D, arrows) and their dendrites (E, arrow) in DMN showing Cx36-puncta localized at a dendro-somatic apposition (D, arrowhead) and at dendro-dendritic appositions (E, arrowheads). (F, G) Images of eGFP$^+$ MNs (F, G, large arrows) and eGFP$^-$ MNs (F, G, small arrows) in the DMN, showing Cx36-puncta along an eGFP$^+$ dendrite in close proximity with a ChAT$^+$/eGFP$^-$ MN somata (F, arrowhead), and Cx36-puncta (G1, G2, arrowheads) between two adjacent eGFP$^+$ (G1, G2, large arrows) and eGFP$^-$ (G1, G2, small arrows) MNs. (H, I) Images of ChAT$^+$ MNs that are eGFP$^-$ in the DMN, showing a large cluster of Cx36-puncta (H, arrowhead) localized at a MN somata (H, arrow), with the cluster shown in the inset, and a similar cluster of Cx36-puncta (I, arrowheads) at an apposition between to eGFP$^-$ MNs (I, arrows).

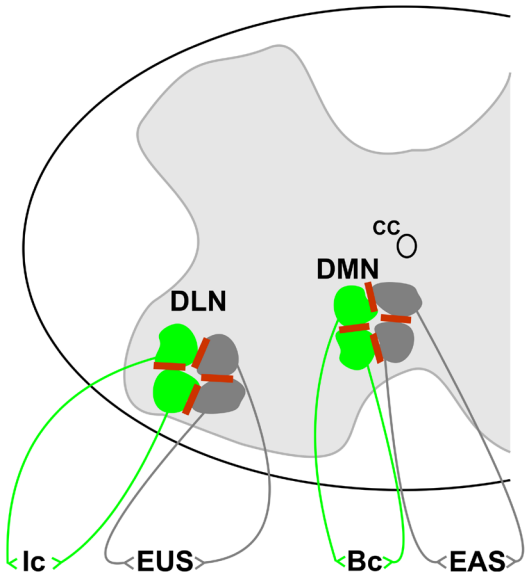

Figure 10. Summary diagram indicating the proposed configuration of electrical synapses mediated by neuronal gap junctions (red bars) linking MN in the DLN and DMN. Sexually dimorphic MNs (green) in these motor nuclei that innervate the ischiocavernosis (Ic) and bulbocavernosus muscle (Bc) couple with each other as well as with sexually non-dimorphic MNs (grey) that innervate the external urethral sphincter (EUS) and the external anal sphincter (EAS), and the non-sexually dimorphic MNs innervating the EUS and EAS are themselves coupled.

Cx36 or whether this represents false-negative eGFP expression in the Cx36^{BAC}::eGFP mice. Nevertheless, given the multiple and diverse functions in which lower lumbar sexually dimorphic muscles and upper lumbar cremaster muscles are engaged, e-coupling of their constituent MNs may be considered in relation to the physiological processes governed by the muscle they innervate.

Musculature supporting sexual behaviour

We have previously speculated on the organization of electrical coupling between the dimorphic vs. non-dimorphic MN populations in the DMN and DLN with respect to patterns of their muscle innervation [32]. This can now be further addressed with: i) our finding of a fortuitous complete segregation of projections by eGFP$^+$ MNs in these nuclei to sexually dimorphic ischiocavernosus and bulbocavernosus muscles, and projections of eGFP$^-$ MNs to the non-dimorphic external anal sphincter and external urethral sphincter muscles; and ii) our observations of Cx36-puncta indicative of electrical synapses formation between eGFP$^+$, between eGFP$^-$ and between eGFP$^+$/eGFP$^-$ motoneuronal elements in both the DMN and DLN. Consideration of these points suggest the occurrence of e-coupling between the dimorphic MNs in each nucleus, between the non-dimorphic MNs in each nucleus and between the dimorphic and non-dimorphic MNs in each nucleus, as depicted in **Figure 10**.

It has been previously suggested that synchronous activity of sexually dimorphic MNs conferred by their e-coupling could be required to maintain concerted action of perineal muscles that support the physiology and behaviour of copulation in males [88]. Indeed, manipulations that allow activation of the urethrogenital reflex in spinalized male rats elicited various features of copulation in the intact male, including penile erection, pelvic muscle activation and ejaculation, and electrophysiological recordings from the pudendal nerve that contains axons of MNs arising from DMN and DLN as well as recordings from the four target muscles of these two motor nuclei revealed that all the

perineal muscle contractions were synchronous [89-91]. The concerted activity of the dimorphic muscles was suggested to be required for erectile and ejaculatory functions, while tonic activity in the sphincter muscles contribute to closure of the external anal and external urethral sphincters during sexual activity [89]. In analogy with the lower lumbar dimorphic motor nuclei, networks of cremaster MNs in males also appear to activate their target musculature during sexual behaviour as reflected by elevation of the testes during ejaculation [92], and strong, fast contractions of the cremaster muscle were suggested to support this process [42, 49]. Like the ischiocavernosus and bulbocavernosus muscles, the cremaster muscle is also activated to elevate the testes during micturition [93] and during threatening behavioural situations where protection of the testes may be required [73]. Further, the more complex sequelae of perineal muscle activity seen in normal male rats during sexual activity [47, 48] suggests that moment-to-moment patterns of coupling between motoneuronal pools in these nuclei may be subject to strict regulation.

Muscles supporting thermoregulation

Besides its support of sexual activity, the cremaster muscle has been more intensively investigated with respect to its contribution to thermoregulation of the testes, which in mammals are kept 2-7°C below body temperature to allow normal spermatogenesis [37, 41-43], and to generation of the cremaster reflex that is elicited by stimulation of the inner pelvic skin area, causing elevation and protection of the testes [44]. Thermoregulation of the testes involves both striated cremaster muscle enveloping the testes and more superficial smooth muscles, where the former serves to control the proximity of the testes to the rest of the body and the latter adjusts scrotal surface area to conserve or dissipate heat. However, less generally known is an equally powerful thermoregulatory system associated with the spermatic cord that, in addition to other structures, contains an arterial and venous plexus providing blood flow to and from the testes, and that is surrounded by portions of cremaster muscle. This plexus performs as a highly efficient counter current heat exchanger, where arterial blood flowing distally is cooled to scrotal temperature and venous return is warmed to body temperature [94, 95]. Thus, blood flow in the spermatic cord is diminished by cremaster muscle contraction upon scrotal cooling and increased by its relaxation upon scrotal warming [96], where the contraction prevents excessive precooling of arterial by venous blood in cold conditions. Because activity in the cremaster muscle is invoked during sexual behaviour to facilitate ejaculation as discussed above and during testicular thermoregulation, it is likely that separate populations of cremaster MNs control different portions of cremaster muscles involved in these somewhat distinct physiological processes, which is further suggested by evidence for differential projections of cremaster MNs to anatomically distinct regions of cremaster muscle [49].

Conclusions

Electrical synapses are generally considered low pass filters because they are especially adept at transmitting currents from cell to cell that are subthreshold for action potential generation [3, 18]. Such current flow serves to equalize the subthreshold depolarization state of neurons in an e-coupled network, such that any excitatory input now enables firing threshold to be reached nearly simultaneously, creating synchronous activity in the network [5, 7, 20, 21]. In the CNS, such synchronous activity impacts the correlated discharge of downstream targets of the e-coupled network. In the case of e-coupled MNs, near simultaneous recruitment of their action potential firing would promote correlated activity of motor units in their target muscles, which is relevant to established principles where greater speed of MNs recruitment is one major contributing factor to rapid muscle force generation [97-100]. Thus, it may be considered that synchronous activity conferred by e-coupling between MNs in DMN and DLN projecting to bulbocavernosus and ischiocavernosus muscles, respectively, would promote high speed and more forceful contraction of these muscles when physiologically required during penile erection, copulation and ejaculation, and such patterns of synchronous activity would be equally essential in the two sphincter muscles receiving projections from e-coupled MNs in these nuclei to prevent micturition and defecation during sexual activity. Similarly, e-coupling between MNs in the cre-

master nucleus projecting to cremaster muscle enveloping the testes would be of benefit for rapid testicular retraction when the protective action of this muscle is called upon, as during fight or flight responses. It remains to be determined whether e-coupling occurs between MNs projecting to cremaster muscle surrounding the spermatic cord and whether such coupling would benefit the testicular thermoregulatory functions of this portion of the cremaster muscle.

Acknowledgements

This work was supported by grants from the Canadian Institutes of Health Research and the Natural Sciences and Engineering Research Council to J.I.N.

Disclosure of conflict of interest

None.

Abbreviations

CNS, central nervous system; ChAT, choline acetyltransferase; Cx36, connexin36; DLN, dorsolateral nucleus; DMN, dorsomedial nucleus; e-coupling, electrical coupling; eGFP, enhanced green fluorescent protein; L, lumbar; MN, motoneurons; PBS, phosphate-buffered saline; TBS, 50 mM Tris-HCl, pH 7.4, 1.5% NaCl; TBST, TBS containing 0.3% Triton X-100; vAChT, vesicular acetylcholine transporter; vglut1, vesicular glutamate transporter-1.

Address correspondence to: Dr. James I Nagy, Department of Physiology and Pathophysiology, Rady Faculty of Health Sciences, Max Rady College of Medicine, University of Manitoba, Basic Medical Sciences Building Room 408, 745 Bannatyne Avenue, Winnipeg, Manitoba R3E 0J9, Canada. Tel: 204-789-3767; Fax: 204-789-3934; E-mail: james.nagy@umanitoba.ca

References

[1] Haas JS, Greenwald CM and Pereda AE. Activity-dependent plasticity of electrical synapses: increasing evidence for its presence and functional roles in the mammalian brain. BMC Cell Biol 2016; 17 Suppl 1: 14.

[2] Nagy JI, Pereda AE and Rash JE. Electrical synapses in mammalian CNS: past eras, present focus and future directions. Biochim Biophys Acta Biomembr 2018; 1860: 102-123.

[3] Alcami P and Pereda AE. Beyond plasticity: the dynamic impact of electrical synapses on neural circuits. Nat Rev Neurosci 2019; 20: 253-271.

[4] Vaughn MJ and Haas JS. On the diverse functions of electrical synapses. Front Cell Neurosci 2022; 16: 910015.

[5] Bennett MV. Gap junctions as electrical synapses. J Neurocytol 1997; 26: 349-366.

[6] Coulon P and Landisman CE. The potential role of gap junctional plasticity in the regulation of state. Neuron 2017; 93: 1275-1295.

[7] Curti S, Davoine F and Dapino A. Function and plasticity of electrical synapses in the mammalian brain: role of non-junctional mechanisms. Biology (Basel) 2022; 11: 81.

[8] Pereda AE, Curti S, Hoge G, Cachope R, Flores CE and Rash JE. Gap junction-mediated electrical transmission: regulatory mechanisms and plasticity. Biochim Biophys Acta 2013; 1828: 134-146.

[9] Pereda AE. Electrical synapses and their functional interactions with chemical synapses. Nat Rev Neurosci 2014; 15: 250-263.

[10] Nagy JI, Bautista W, Blakley B and Rash JE. Morphologically mixed chemical-electrical synapses formed by primary afferents in rodent vestibular nuclei as revealed by immunofluorescence detection of connexin36 and vesicular glutamate transporter-1. Neuroscience 2013; 252: 468-488.

[11] Nagy JI, Pereda AE and Rash JE. On the occurrence and enigmatic functions of mixed (chemical plus electrical) synapses in the mammalian CNS. Neurosci Lett 2019; 695: 53-64.

[12] Rash JE, Kamasawa N, Vanderpool KG, Yasumura T, O'Brien J, Nannapaneni S, Pereda AE and Nagy JI. Heterotypic gap junctions at glutamatergic mixed synapses are abundant in goldfish brain. Neuroscience 2015; 285: 166-193.

[13] Pereda AE and Bennett MVL. Electrical synapses in fishes: their relevance to synaptic transmission. In: Network Functions and Plasticity; perspectives from studying neuronal electrical coupling in microcircuits. NY: Academic Press; 2017. pp. 161-181.

[14] Korn H, Sotelo C and Crepel F. Electronic coupling between neurons in the rat lateral vestibular nucleus. Exp Brain Res 1973; 16: 255-275.

[15] Ixmatlahua DJ, Vizcarra B, Gómez-Lira G, Romero-Maldonado I, Ortiz F, Rojas-Piloni G and Gutiérrez R. Neuronal glutamatergic network electrically wired with silent but activatable gap junctions. J Neurosci 2020; 40: 4661-4672.

[16] O'Brien J. The ever-changing electrical synapse. Curr Opin Neurobiol 2014; 29: 64-72.

[17] O'Brien J. Design principles of electrical synaptic plasticity. Neurosci Lett 2019; 695: 4-11.
[18] Curti S and O'Brien J. Characteristics and plasticity of electrical synaptic transmission. BMC Cell Biol 2016; 17 Suppl 1: 13.
[19] Connors BW and Long MA. Electrical synapses in the mammalian brain. Annu Rev Neurosci 2004; 27: 393-418.
[20] Connors BW. Electrical signaling with neuronal gap junctions. In: Harris A, Locke D, editors. Connexins: A Guide. Springer: Humana Press; 2009. pp. 143-164.
[21] Connors BW. Synchrony and so much more: diverse roles for electrical synapses in neural circuits. Dev Neurobiol 2017; 77: 610-624.
[22] Nagy JI, Lynn BD, Senecal JMM and Stecina K. Connexin36 expression in primary afferent neurons in relation to the axon reflex and modality coding of somatic sensation. Neuroscience 2018; 383: 216-234.
[23] Recabal-Beyer AJ, Senecal JMM, Senecal JEM, Lynn BD and Nagy JI. On the organization of connexin36 expression in electrically coupled cholinergic V0c neurons (partition cells) in the spinal cord and their C-terminal innervation of motoneurons. Neuroscience 2022; 485: 91-115.
[24] Recabal-Beyer A, Tavakoli H, Senecal JMM, Stecina K and Nagy JI. Interrelationships between spinal sympathetic preganglionic neurons, autonomic systems and electrical synapses formed by connexin36-containing gap junctions. Neuroscience 2023; 523: 31-46.
[25] Hinckley CA and Ziskind-Conhaim L. Electrical coupling between locomotor-related excitatory interneurons in the mammalian spinal cord. J Neurosci 2006; 26: 8477-8483.
[26] Wilson JM, Cowan AI and Brownstone RM. Heterogeneous electrotonic coupling and synchronization of rhythmic bursting activity in mouse Hb9 interneurons. J Neurophysiol 2007; 98: 2370-2381.
[27] Lall VK, Dutschmann M, Deuchars J and Deuchars SA. The anti-malarial drug mefloquine disrupts central autonomic and respiratory control in the working heart brainstem preparation of the rat. J Biomed Sci 2012; 19: 103.
[28] Lall VK, Bruce G, Voytenko L, Drinkhill M, Wellershaus K, Willecke K, Deuchars J and Deuchars SA. Physiologic regulation of heart rate and blood pressure involves connexin 36-containing gap junctions. FASEB J 2017; 31: 3966-3977.
[29] Bautista W, Nagy JI, Dai Y and McCrea DA. Requirement of neuronal connexin36 in pathways mediating presynaptic inhibition of primary afferents in functionally mature mouse spinal cord. J Physiol 2012; 590: 3821-3839.
[30] Matsumoto A, Arnold AP, Zampighi GA and Micevych PE. Androgenic regulation of gap junctions between motoneurons in the rat spinal cord. J Neurosci 1988; 8: 4177-4183.
[31] Matsumoto A, Arnold AP and Micevych PE. Gap junctions between lateral spinal motoneurons in the rat. Brain Res 1989; 495: 362-366.
[32] Bautista W and Nagy JI. Connexin36 in gap junctions forming electrical synapses between motoneurons in sexually dimorphic motor nuclei in spinal cord of rat and mouse. Eur J Neurosci 2014; 39: 771-787.
[33] Singhal P, Senecal JMM, Senecal JEM, Silwal P, Lynn BD and Nagy JI. Characteristics of electrical synapses, C-terminals and small-conductance Ca2+ activated potassium channels in the sexually dimorphic cremaster motor nucleus in spinal cord of mouse and rat. Neuroscience 2023; 521: 58-76.
[34] Breedlove SM and Arnold AP. Hormone accumulation in a sexually dimorphic motor nucleus of the rat spinal cord. Science 1980; 210: 564-566.
[35] Jordan CL, Breedlove SM and Arnold AP. Sexual dimorphism and the influence of neonatal androgen in the dorsolateral motor nucleus of the rat lumbar spinal cord. Brain Res 1982; 249: 309-314.
[36] Kojima M and Sano Y. Sexual differences in the topographical distribution of serotonergic fibers in the anterior column of rat lumbar spinal cord. Anat Embryol (Berl) 1984; 170: 117-121.
[37] Nagy JI and Senba E. Neural relations of cremaster motoneurons, spinal cord systems and the genitofemoral nerve in the rat. Brain Res Bull 1985; 15: 609-627.
[38] McKenna KE and Nadelhaft I. The organization of the pudendal nerve in the male and female rat. J Comp Neurol 1986; 248: 532-549.
[39] Newton BW and Hamill RW. Target regulation of the serotonin and substance P innervation of the sexually dimorphic cremaster nucleus. Brain Res 1989; 485: 149-156.
[40] Schroder HD. Organization of the motoneurons innervating the pelvic muscles of the male rat. J Comp Neurol 1980; 192: 567-587.
[41] Kojima M and Ohe H. Experimental study on the regulation of testicular function by the cremaster reflex in rats. Tohoku J Exp Med 1986; 150: 175-180.
[42] Lucio RA, Flores-Rojas G, Aguilar F, Zempoalteca R, Pacheco P and Velazquez-Moctezuma J. Effects of genitofemoral nerve transection on copulatory behavior and fertility in male rats. Physiol Behav 2001; 73: 487-492.
[43] Sengul G and Ertekin C. Human cremaster muscle and cremasteric reflex: a comprehensive review. Clin Neurophysiol 2020; 131: 1354-1364.
[44] Schwarz GM and Hirtler L. The cremasteric reflex and its muscle - a paragon of ongoing sci-

entific discussion: a systematic review. Clin Anat 2017; 30: 498-507.
[45] Hart BL and Melese-D'Hospital PY. Penile mechanisms and the role of the striated penile muscles in penile reflexes. Physiol Behav 1983; 31: 807-813.
[46] Elmore LA and Sachs BD. Role of the bulbospongiosus muscles in sexual behavior and fertility in the house mouse. Physiol Behav 1988; 44: 125-129.
[47] Holmes GM, Chapple WD, Leipheimer RE and Sachs BD. Electromyographic analysis of male rat perineal muscles during copulation and reflexive erections. Physiol Behav 1991; 49: 1235-1246.
[48] Schmidt MH and Schmidt HS. The ischiocavernosus and bulbospongiosus muscles in mammalian penile rigidity. Sleep 1993; 16: 171-183.
[49] Zempoalteca R, Martinez-Gomez M, Hudson R, Cruz Y and Lucio RA. An anatomical and electrophysiological study of the genitofemoral nerve and some of its targets in the male rat. J Anat 2002; 201: 493-505.
[50] Nagy JI and Rash JE. Cx36, Cx43 and Cx45 in mouse and rat cerebellar cortex: species-specific expression, compensation in Cx36 null mice and co-localization in neurons vs. glia. Eur J Neurosci 2017; 46: 1790-1804.
[51] Curti S, Hoge G, Nagy JI and Pereda AE. Synergy between electrical coupling and membrane properties promotes strong synchronization of neurons of the mesencephalic trigeminal nucleus. J Neurosci 2012; 32: 4341-4359.
[52] Rubio ME and Nagy JI. Connexin36 expression in major centers of the auditory system in the CNS of mouse and rat: evidence for neurons forming purely electrical synapses and morphologically mixed synapses. Neuroscience 2015; 303: 604-629.
[53] Dapson RW. Glyoxal fixation: how it works and why it only occasionally needs antigen retrieval. Biotech Histochem 2007; 82: 161-166.
[54] Richter KN, Revelo NH, Seitz KJ, Helm MS, Sarkar D, Saleeb RS, D'Este E, Eberle J, Wagner E, Vogl C, Lazaro DF, Richter F, Coy-Vergara J, Coceano G, Boyden ES, Duncan RR, Hell SW, Lauterbach MA, Lehnart SE, Moser T, Outeiro TF, Rehling P, Schwappach B, Testa I, Zapiec B and Rizzoli SO. Glyoxal as an alternative fixative to formaldehyde in immunostaining and super-resolution microscopy. EMBO J 2018; 37: 139-159.
[55] Konno K, Yamasaki M, Miyazaki T and Watanabe M. Glyoxal fixation: an approach to solve immunohistochemical problem in neuroscience research. Sci Adv 2023; 9: eadf7084.
[56] Dail WG and Sachs BD. The ischiourethralis muscle of the rat: anatomy, innervation, and function. Anat Rec 1991; 229: 203-208.
[57] Yang Y, Wu X, Leng Q, Su W, Wang S, Xing R, Zhou X, Lv D, Li B and Mao X. Microstructures of the spermatic cord with three-dimensional reconstruction of sections of the cord and application to varicocele. Syst Biol Reprod Med 2020; 66: 216-222.
[58] Van Keuren ML, Gavrilina GB, Filipiak WE, Zeidler MG and Saunders TL. Generating transgenic mice from bacterial artificial chromosomes: transgenesis efficiency, integration and expression outcomes. Transgenic Res 2009; 18: 769-785.
[59] Parysek LM and Goldman RD. Distribution of a novel 57 kDa intermediate filament (IF) protein in the nervous system. J Neurosci 1988; 8: 555-563.
[60] Clarke WT, Edwards B, McCullagh KJ, Kemp MW, Moorwood C, Sherman DL, Burgess M and Davies KE. Syncoilin modulates peripherin filament networks and is necessary for large-calibre motor neurons. J Cell Sci 2010; 123: 2543-2552.
[61] Zhao J and Liem RK. α-Internexin and peripherin: expression, assembly, functions, and roles in disease. Methods Enzymol 2016; 568: 477-507.
[62] Watson C, Paxinos G and Kayalioglu G. The Spinal Cord: A Christopher and Dana Reeve Foundation Text and Atlas. Amsterdam: Academic Press; 2009.
[63] Ueyama T, Arakawa H and Mizuno N. Central distribution of efferent and afferent components of the pudendal nerve in rat. Anat Embryol (Berl) 1987; 177: 37-49.
[64] Rose RD and Collins WF 3rd. Crossing dendrites may be a substrate for synchronized activation of penile motoneurons. Brain Res 1985; 337: 373-377.
[65] Forger NG, Howell ML, Bengston L, MacKenzie L, DeChiara TM and Yancopoulos GD. Sexual dimorphism in the spinal cord is absent in mice lacking the ciliary neurotrophic factor receptor. J Neurosci 1997; 17: 9605-9612.
[66] Zuloaga DG, Morris JA, Monks DA, Breedlove SM and Jordan CL. Androgen-sensitivity of somata and dendrites of spinal nucleus of the bulbocavernosus (SNB) motoneurons in male C57BL6J mice. Horm Behav 2007; 51: 207-212.
[67] Sengelaub DR and Arnold AP. Development and loss of early projections in a sexually dimorphic rat spinal nucleus. J Neurosci 1986; 6: 1613-1620.
[68] Breedlove SM. Cellular analyses of hormone influence on motoneuronal development and function. J Neurobiol 1986; 17: 157-176.
[69] Sengelaub DR and Forger NG. The spinal nucleus of the bulbocavernosus: firsts in androgen-dependent neural sex differences. Horm Behav 2008; 53: 596-612.

[70] Wagner CK and Clemens LG. Anatomical organization of the sexually dimorphic perineal neuromuscular system in the house mouse. Brain Res 1989; 499: 93-100.
[71] Kojima M, Takeuchi Y, Kawata M and Sano Y. Motoneurons innervating the cremaster muscle of the rat are characteristically densely innervated by serotoninergic fibers as revealed by combined immunohistochemistry and retrograde fluorescence DAPI-labelling. Anat Embryol (Berl) 1983; 168: 41-49.
[72] Newton BW. Peptidergic innervation of the cremaster nucleus. I. A sexually dimorphic population of substance P-containing intraspinal neurons exists in the substance P pathway to the rat cremaster nucleus. Brain Res 1990; 537: 187-196.
[73] Li X, Olson C, Lu S, Kamasawa N, Yasumura T, Rash JE and Nagy JI. Neuronal connexin36 association with zonula occludens-1 protein (ZO-1) in mouse brain and interaction with the first PDZ domain of ZO-1. Eur J Neurosci 2004; 19: 2132-2146.
[74] Kamasawa N, Furman CS, Davidson KG, Sampson JA, Magnie AR, Gebhardt BR, Kamasawa M, Yasumura T, Zumbrunnen JR, Pickard GE, Nagy JI and Rash JE. Abundance and ultrastructural diversity of neuronal gap junctions in the OFF and ON sublaminae of the inner plexiform layer of rat and mouse retina. Neuroscience 2006; 142: 1093-1117.
[75] Bautista W, McCrea DA and Nagy JI. Connexin36 identified at morphologically mixed chemical/electrical synapses on trigeminal motoneurons and at primary afferent terminals on spinal cord neurons in adult mouse and rat. Neuroscience 2014; 263: 159-180.
[76] Rash JE, Staines WA, Yasumura T, Patel D, Furman CS, Stelmack GL and Nagy J. Immunogold evidence that neuronal gap junctions in adult rat brain and spinal cord contain connexin-36 but not Cx32 or Cx43. Proc Natl Acad Sci U S A 2000; 97: 7573-7578.
[77] Rash JE, Yasumura T, Dudek FE and Nagy JI. Cell-specific expression of connexins and evidence of restricted gap junctional coupling between glial cells and between neurons. J Neurosci 2001; 21: 1983-2000.
[78] Rash JE, Pereda A, Kamasawa N, Furman CS, Yasumura T, Davidson KG, Dudek FE, Olson C, Li X and Nagy JI. High-resolution proteomic mapping in the vertebrate central nervous system: close proximity of connexin35 to NMDA glutamate receptor clusters and co-localization of connexin36 with immunoreactivity for zonula occludens protein-1 (ZO-1). J Neurocytol 2004; 33: 131-151.
[79] Rash JE, Olson CO, Pouliot WA, Davidson KG, Yasumura T, Furman CS, Royer S, Kamasawa N, Nagy JI and Dudek FE. Connexin36 vs. connexin32, "miniature" neuronal gap junctions, and limited electrotonic coupling in rodent suprachiasmatic nucleus. Neuroscience 2007; 149: 350-371.
[80] Rash JE, Olson CO, Davidson KG, Yasumura T, Kamasawa N and Nagy JI. Identification of connexin36 in gap junctions between neurons in rodent locus coeruleus. Neuroscience 2007; 147: 938-956.
[81] Fukuda T. Network architecture of gap junction-coupled neuronal linkage in the striatum. J Neurosci 2009; 29: 1235-1243.
[82] Shigematsu N, Nishi A and Fukuda T. Gap junctions interconnect different subtypes of parvalbumin-positive interneurons in barrels and septa with connectivity unique to each subtype. Cereb Cortex 2019; 29: 1414-1429.
[83] Nagy JI. Evidence for connexin36 localization at hippocampal mossy fiber terminals suggesting mixed chemical/electrical transmission by granule cells. Brain Res 2012; 1487: 107-122.
[84] Collins WF and Erichsen JT. Direct excitatory interactions between rat penile motoneurons. Soc Neurosci Abstr 1988; 14: 181.
[85] Jankowska E, Padel Y and Zarzecki P. Crossed disynaptic inhibition of sacral motoneurones. J Physiol 1978; 285: 425-444.
[86] Taylor DC, Korf HW and Pierau FK. Distribution of sensory neurons of the pudendal nerve in the dorsal root ganglia and their projection to the spinal cord. Horseradish-peroxidase studies in the rat. Cell Tissue Res 1982; 226: 555-564.
[87] Alvarez FJ, Villalba RM, Zerda R and Schneider SP. Vesicular glutamate transporters in the spinal cord, with special reference to sensory primary afferent synapses. J Comp Neurol 2004; 472: 257-280.
[88] Coleman AM and Sengelaub DR. Patterns of dye coupling in lumbar motor nuclei of the rat. J Comp Neurol 2002; 454: 34-41.
[89] McKenna KE and Nadelhaft I. The pudendopudendal reflex in male and female rats. J Auton Nerv Syst 1989; 27: 67-77.
[90] Marson L and McKenna KE. The identification of a brainstem site controlling spinal sexual reflexes in male rats. Brain Res 1990; 515: 303-308.
[91] McKenna KE, Chung SK and McVary KT. A model for the study of sexual function in anesthetized male and female rats. Am J Physiol 1991; 261: R1276-85.
[92] Hollinshead WH and Rosse C. The inguinal and femoral canals, the scrotum. Textbook of Anatomy, 4th edition. Philadelphia: Harper and Row; 1985. pp. 722.
[93] Cruz Y and Downie JW. Sexually dimorphic micturition in rats: relationship of perineal muscle

activity to voiding pattern. Am J Physiol Regul Integr Comp Physiol 2005; 289: R1307-1318.
[94] Waites GMH. Temperature regulation and the testis. In: Johnson AD, Gomes WR, Vandemark NL, editors. The Testes. Vol I, Deveopment, Anatomy and Physiology. New York: Academic Press; 1970. pp. 241-279.
[95] Shafik A. Thermoregulatory apparatus of the testicle. A review. Urology 1974; 41: 473-479.
[96] Shafik A. The cremasteric muscle. In: Johnson AD, Gomes WR, Vandemark NL, editors. The Testis. Vol IV. Advances in Physiology, Biochemistry and Function. New York: Academic Press; 1977. pp. 481-489.
[97] Enjin A, Rabe N, Nakanishi ST, Vallstedt A, Gezelius H, Memic F, Lind M, Hjalt T, Tourtellotte WG, Bruder C, Eichele G, Whelan PJ and Kullander K. Identification of novel spinal cholinergic genetic subtypes disclose chodl and Pitx2 as markers for fast motor neurons and partition cells. J Comp Neurol 2010; 518: 2284-2304.
[98] Duchateau J and Baudry S. Maximal discharge rate of motor units determines the maximal rate of force development during ballistic contractions in human. Front Hum Neurosci 2014; 8: 234.
[99] Enoka RM and Duchateau J. Rate coding and the control of muscle force. Cold Spring Harb Perspect Med 2017; 7: a029702.
[100] Del Vecchio A, Negro F, Holobar A, Casolo A, Folland JP, Felici F and Farina D. You are as fast as your motor neurons: speed of recruitment and maximal discharge of motor neurons determine the maximal rate of force development in humans. J Physiol 2019; 597: 2445-2456.